



Global ship track distribution and radiative forcing from 1 year of AATSR data

Mathias Schreier,^{1,2} Hermann Mannstein,² Veronika Eyring,² and Heinrich Bovensmann¹

Received 11 May 2007; accepted 9 August 2007; published 13 September 2007.

[1] One year of ENVISAT-AATSR (Advanced Along Track Scanning Radiometer) satellite data is analyzed to derive a global distribution of ship tracks and their radiative forcing (RF). Ship tracks are changes in cloud reflectance, visible in satellite data, and result from the emission of aerosols and their precursors by ships into the clean marine boundary layer. An algorithm is presented that extracts scenes dominated by low clouds over the oceans that are susceptible to be affected by ship emissions. These selected cloud scenes are used to examine ship tracks on a global scale via visual analysis. The results show a high temporal variability of ship track occurrence with peak values in July. They also show a high spatial variability with peak values in the North Pacific Ocean and on the west coast of southern Africa, correlated with high ship traffic and frequent low cloud occurrence in regions of cold upwelling ocean currents. The analysis of backscattered radiation at top of the atmosphere (TOA) compared to the surrounding area reveals enhanced backscattering with values between 0 and 100 Wm^{-2} . For particular regions on the west coast of North America, the annual mean RF due to ship tracks estimated by the changes in backscattered radiation at TOA can be up to -50 mWm^{-2} . The global annual mean RF due to ship tracks is small (-0.4 to -0.6 mWm^{-2}) and negligible compared to previous global model estimates on the total indirect aerosol effect and RF contributions of other ship emissions. **Citation:** Schreier, M., H. Mannstein, V. Eyring, and H. Bovensmann (2007), Global ship track distribution and radiative forcing from 1 year of AATSR data, *Geophys. Res. Lett.*, 34, L17814, doi:10.1029/2007GL030664.

1. Introduction

[2] Emissions from international shipping contribute significantly to the total budget of anthropogenic emissions from the transportation sector [Eyring *et al.*, 2005]. The total emissions of particles and their precursors are even higher than those from road-traffic, because of the high sulfur content of the fuel burned in marine diesel engines today. At present, there are regional attempts to regulate sulfur emissions from shipping (e.g. the sulfur emission control area (SECA) in the Baltic Sea) but only marginal regulations for offshore ship traffic [Entec UK Limited, 2002].

¹Institute for Environmental Physics, University of Bremen, Bremen, Germany.

²Institut für Physik der Atmosphäre, Deutsches Zentrum für Luft- und Raumfahrt, Oberpfaffenhofen, Germany.

[3] In the clean marine environment, the amount of cloud condensation nuclei (CCN) is small [O'Dowd *et al.*, 1997] and low marine clouds usually have large droplet radii combined with low droplet numbers [Han *et al.*, 1998] compared to continental clouds. Emissions of aerosols and their precursors by ships result in a high amount of additional CCNs and can possibly lead to a change of the optical and microphysical properties of clouds [Durkee *et al.*, 2000; Platnick *et al.*, 2000]. This results in an increased backscattering of the cloud layer, known as indirect aerosol effect [Twomey *et al.*, 1968; Albrecht, 1989; Rosenfeld *et al.*, 2006].

[4] Previous modeling studies indicate a potentially large indirect aerosol effect due to shipping [Capaldo *et al.*, 1999]. The satellite data analysis presented here is restricted to the visually detectable impact of ship emissions on clouds, identified by elongated structures in satellite images, known as ship tracks. Ship tracks have been shown to change the radiation budget on a local scale [Schreier *et al.*, 2006]. Thus, there is considerable interest to estimate their radiative impact on global scale. An algorithm is applied to extract scenes dominated by marine low clouds susceptible for ship emissions and development of ship tracks. From this analysis, the global amount of ship tracks from one year of AATSR (Advanced Along Track Scanning Radiometer) satellite data and the resulting radiative forcing (RF) for the year 2004 is estimated.

2. Retrieval of Ship Tracks

[5] The amount and coverage of ship tracks is estimated from global nadir measurements of the AATSR [Llewellyn-Jones *et al.*, 2001] instrument aboard the polar orbiting European ENVISAT satellite for the year 2004. The spatial resolution of this instrument hereby is 1 km and the scan-width is 512 km. 14.4 orbits per day result in a re-visiting time of approximately 5.4 days at the equator for the late morning ($\sim 10:00$ local time).

[6] Ship tracks covered by higher clouds do not affect the net solar radiation by increased backscattering. The remaining relevant ship tracks are usually either embedded in low clouds or can be found in the vicinity of them. Therefore we use a three-step approach to identify ship tracks in satellite data: first we automatically select scenes with at least 20% coverage of very low clouds in the marine boundary layer (VLC), where 4161 scenes are selected as VLC scenes over the ocean in 2004 (section 2.1). This reduces the data amount by 98%. Then we sort out those scenes without ship tracks (3830 scenes) and analyzed the remaining scenes (331 scenes) for possible ship tracks (section 2.2). Finally, the cloud optical properties of the ship tracks and the

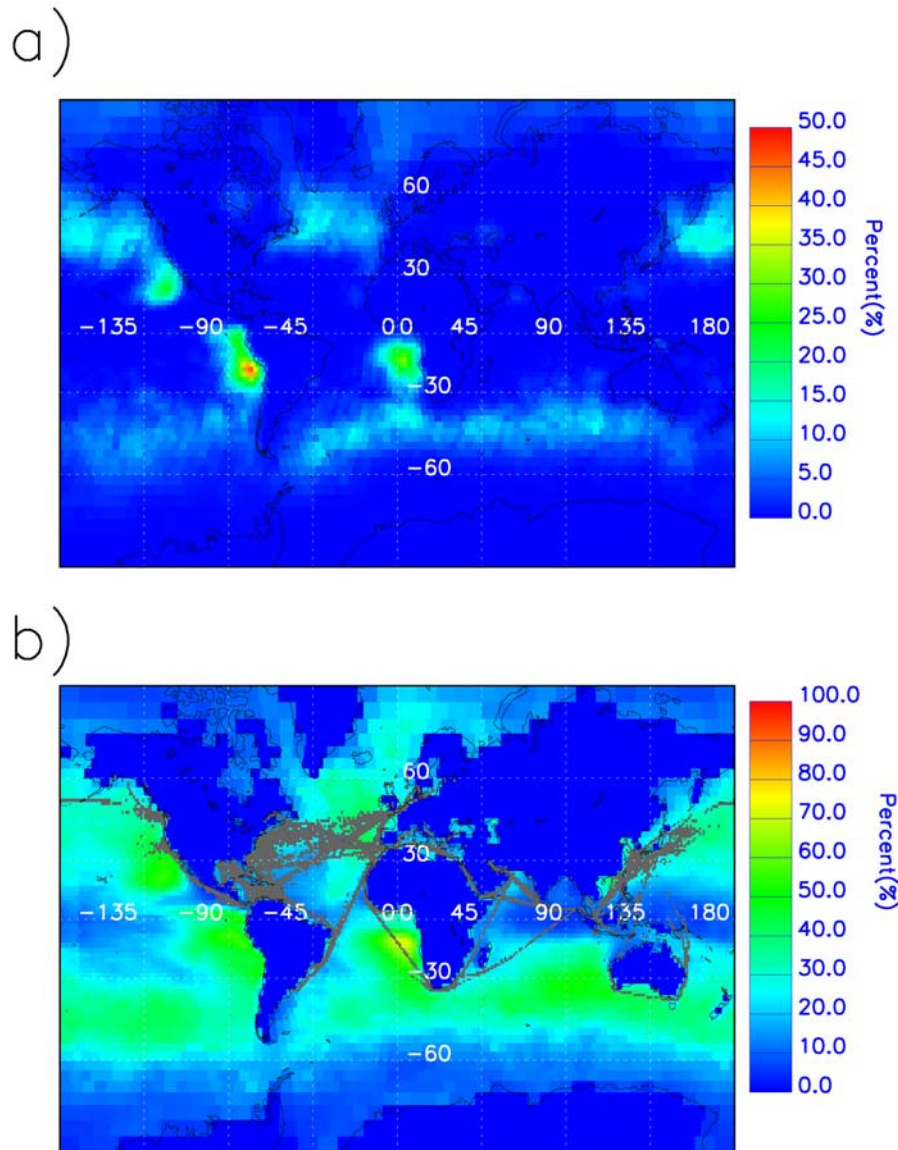


Figure 1. (a) Annual mean global cover of very low clouds over the ocean in % derived from AATSR data in comparison with (b) clouds below 680 hPa over the ocean derived from ISCCP data in 2004. Grey areas indicate high vessel densities. Note that the scale goes to 50% in Figure 1a and to 100% in Figure 1b.

surrounding area within the selected scenes are used to estimate radiative forcing due to ship tracks (section 2.3).

2.1. Global Coverage of Low Marine Clouds

[7] We use auxiliary geophysical data to select scenes over the ocean areas and on sun position to reduce the data amount to daylight scenes, as ship tracks will not have a substantial impact on the net radiation at night. To select scenes with low clouds over the ocean we applied the following criteria: (1) reflectance for $0.87 \mu\text{m}$ larger than 0.2, and (2) temperature for $11 \mu\text{m}$ less than 4 K colder than local sea surface brightness temperature (approximated by the maximum temperatures of each image line).

[8] Criterion 1 is applied to distinguish clouds from cloud-free ocean. Criterion 2 is needed to estimate the cloud top height. It uses a temperature difference of 4 K between the cloud and the maximum temperature, which usually

corresponds to the sea surface temperature. Clouds susceptible for ship tracks are very low [Durkee *et al.*, 2000; Platnick *et al.*, 2000] and assuming a wet adiabatic lapse rate of $-0.6 \text{ K}/100 \text{ m}$, a maximum temperature difference of about 4 K between cloud top temperature and sea surface temperature results in a cloud top height of $\sim 700 \text{ m}$. If 256 successive lines fulfill criteria 1 and 2 by more than 20%, this part of the orbit (plus additional 256 lines on both ends) is selected as VLC scene for further analysis. Our automated selection of scenes is verified by a thorough analysis of 1% of the complete satellite data (4 days, one for each season), showing a ship track detection efficiency of 70% when reducing the original data by 98%.

[9] To validate the algorithm, we compare the global coverage pattern of VLC that result from our analysis to the ISCCP (International Satellite Cloud Climatology Project, Rossow and Schiffer [1991]) data base. From the ISCCP

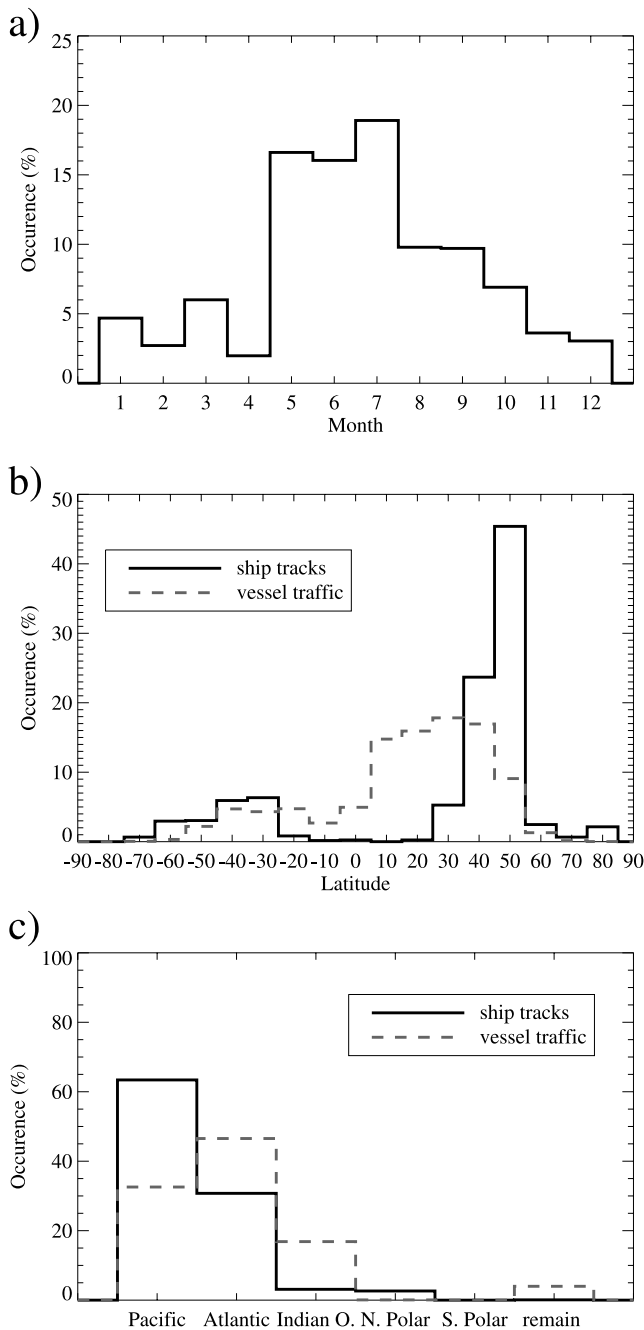


Figure 2. (a) Global and monthly mean ship track occurrence in % versus months for 2004. (b) Latitudinal distribution of annual mean ship track occurrence with vessel traffic densities from AMVER superimposed. (c) Same as in Figure 2b, but for different regions.

data set, it is possible to deduce daytime low clouds over the ocean. ISCCP low clouds are defined within the altitude range from 1000 to 680 hPa, a much wider range than represented by VLC, leading to higher cloud coverage. The retrieved AATSR data are sampled into the ISCCP grid boxes ($\sim 275 \times 275$ km).

[10] The maxima in VLC coverage derived from AATSR data in 2004 are found in the sub-tropical latitudes at the west

coasts of southern Africa, South America, and North America (Figure 1a). In these regions cold upwelling ocean currents lead to a stable atmospheric boundary layer in combination with a low coverage by higher level clouds. In both hemispheres there is also a broad belt of increased coverage between 30° and 60° , resulting from the global Hadley circulation. A very similar pattern is found in the low cloud fraction of ISCCP data from the year 2004 (Figure 1b). But, as expected, the amount of VLC in the AATSR data is much smaller than in ISCCP, as the temperature criterion selects clouds below 900 hPa whereas the boundary pressure level for the ISCCP low clouds is 680 hPa.

2.2. Global Ship Track Distribution

[11] To derive a global distribution, ship tracks are analyzed visually from a visible-infrared color composite (0.67, 0.87, and $12.0 \mu\text{m}$) and a near-infrared combination (3.7, 12.0, and $1.6 \mu\text{m}$) of the VLC scenes. In a first step, the scenes are screened for ship tracks and scenes dominated by sea-ice, which is also detected by the algorithm, are eliminated. Then the number of ship tracks in the VLC scenes is counted and the resulting distribution for ship track occurrence is normalized to 100%. The frequency of occurrence for ship tracks is compared to the relative vessel traffic density from the Automated Mutual-assistance Vessel Rescue system (AMVER) data set [Endresen *et al.*, 2003], see Figure 2. Compared to the strong seasonal cycle in ship track occurrence (Figure 2a), the seasonal variation in vessel traffic densities is small (see e.g., <http://www.amver.com>). On the global average the number of ship tracks is small between January and April in 2004, but there is a strong increase in May and a maximum from May to July, decreasing continuously again over the following months. Figure 2b shows that in the annual mean the highest occurrence of ship tracks is located between 35° and 55°N . There is also a secondary maximum on the Southern Hemisphere (25° – 45°S). The maximum in vessel traffic densities in the AMVER data is located at lower latitudes. Nearly two third of all ship tracks are found over the Pacific, and almost one-third over the Atlantic (Figure 2c). Only a few ship tracks are detected in the Indian Ocean although the vessel traffic densities indicate high ship traffic in this region.

[12] In a second step the number of pixels for each ship track in a given VLC scene is marked manually. The total number of pixels is weighted by the number of possible observations in order to derive the global distribution of ship track coverage for 2004 (Figure 3a). Most ship tracks occur over the North Pacific Ocean and at the west coast of southern Africa with an annual mean coverage above 0.1%. Values up to 0.05% are found over the Northern Atlantic. This is consistent with the occurrence of very low clouds combined with high vessel traffic densities. Correlation of the ship track coverage with the product of vessel traffic density times very low cloud coverage shows a correlation coefficient of 0.53. Thus, VLC cover and vessel traffic density are important for the formation of ship tracks, but other factors such as uncertainties in the AMVER data, boundary layer height and stability also play a role.

2.3. Radiative Forcing

[13] The observed ship tracks indicate a high variability not only in size but also in backscattering. Some ship tracks

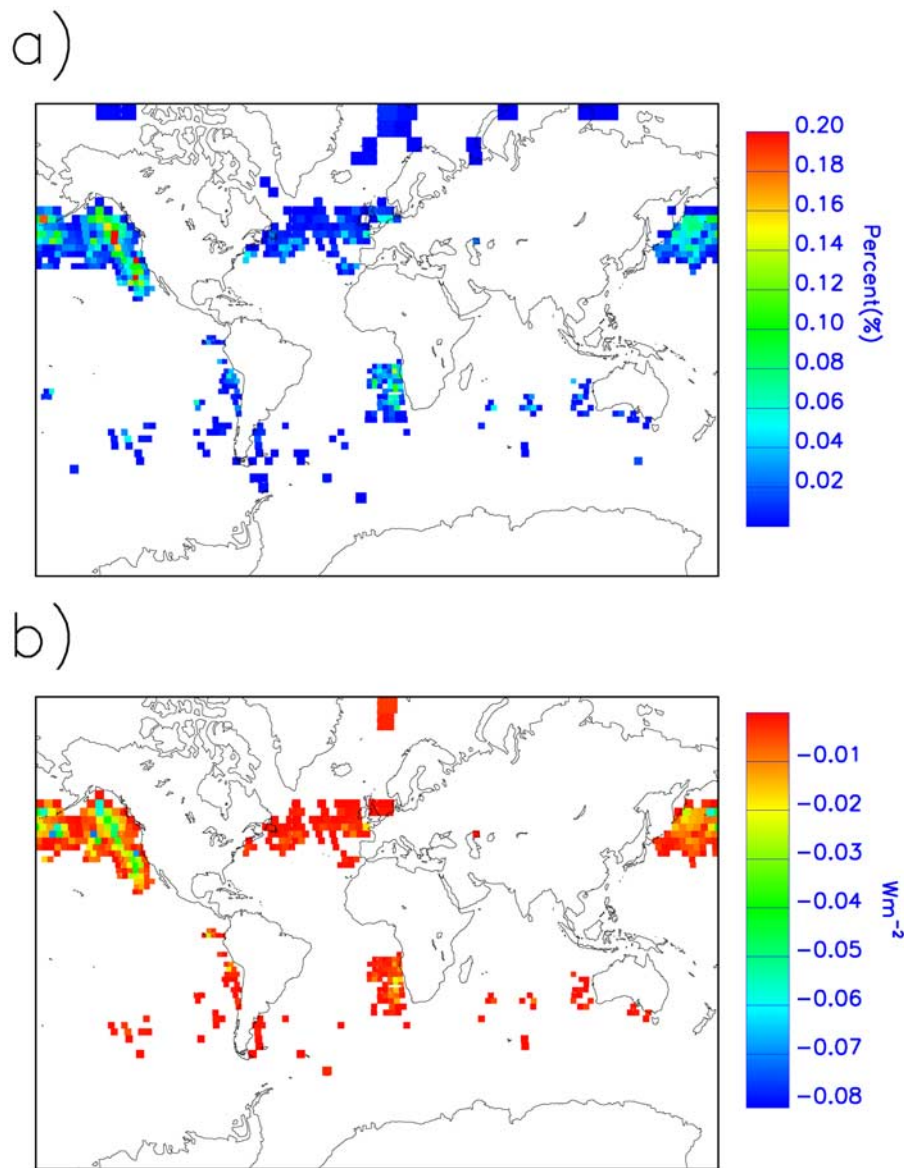


Figure 3. (a) Annual mean coverage distribution of ship tracks and (b) resulting RF distribution due to ship tracks in Wm^{-2} in 2004.

appear within stratus or stratocumulus fields as slight modifications of the existing cloud layer and are detectable mainly in the near infrared channel, which indicates a lower effective radius of the droplets, as explained by *Twomey et al.* [1968]. Others are visible under almost cloud free conditions or indicate possible drizzle suppression as explained by *Albrecht* [1989] and changes in convective pattern as shown by *Rosenfeld et al.* [2006]. The high variability of ship tracks results in a high variation of their radiative behavior. Therefore, in the third step the cloud optical properties like effective radius and cloud optical thickness are calculated for each individual pixel using a combination of the SACURA method (Semi-Analytical Cloud Retrieval Algorithm [*Kokhanovsky et al.*, 2003]) and a look-up-table-approach calculated with the libRadtran package [*Mayer and Kylling*, 2005] as described by *Schreier et al.* [2006]. Using these cloud optical parameters, the backscattered radiative flux at TOA is calculated for the possible solar

zenith angles, depending on the latitude and season, within the ship tracks and in the surrounding region. The RF due to a single ship track is calculated from the difference between the average reflected and emitted fluxes from ship tracks and the area free of ship tracks within a distance of 10 km from the ship track as a substitute for the background conditions. The local RF for each grid box is calculated by multiplying the increased backscattered radiative flux of the ship tracks with the coverage of ship tracks as retrieved in section 2.2 in each individual area. The ENVISAT overpass covers only the conditions on late morning. Therefore, we use the optical properties of the ship tracks at $\sim 10:00$ local time to calculate the RF for 13 different sun positions (representative for 06:00 to 18:00 local time). This RF at TOA is below 40 Wm^{-2} in most cases, but some individual ship tracks in otherwise almost cloud free surrounding can cause a change of more than 100 Wm^{-2} (Figure 4).

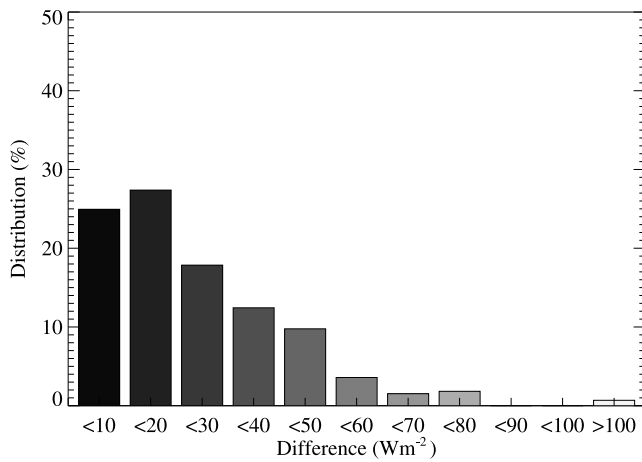


Figure 4. Distribution of mean radiative change in Wm^{-2} compared to surrounding resulting from increased backscattering due to ship tracks calculated as 12 hour average (from 06:00 to 18:00 local time).

[14] Annual mean RF due to ship tracks up to -0.05 Wm^{-2} are found in some regions in the North Pacific Ocean and west of southern Africa (Figure 3b). In the Southern Hemisphere the RF due to ship tracks is generally small, except at the west coasts of southern Africa and South America. The global average RF results from averaging over the whole globe and is summarized in Table 1. Maximum changes of the radiation budget occur in the Northern Hemisphere in summer. The resulting global annual mean RF due to ship tracks is -0.4 mWm^{-2} .

[15] A sensitivity analysis of the RF calculations showed, that the main errors result from the uncertainties in the cloud properties retrieval [Kokhanovsky et al., 2003; Nakajima and King, 1990], but there are also uncertainties resulting from the radiative transfer calculation [Mayer and Kylling, 2005] or the independent-pixel approximation [Cahalan et al., 1994]. The resulting error range from this analysis for the RF calculations is estimated as $\pm 40\%$. Including the potential statistical loss of 30% of all ship tracks (see section 2.1), the global annual mean RF due to ship tracks is -0.4 to $-0.6 \text{ mWm}^{-2} \pm 40\%$. This value is small and negligible compared to previous global model estimates on the RF contributions of other ship emissions [Eyring et al., 2007; Capaldo et al., 1999] and compared to the overall anthropogenic RF [Intergovernmental Panel on Climate Change, 2007].

Table 1. Seasonal Variation of Global RF Due to Ship Tracks for 2004

Season	TOA Global, mWm^{-2}	TOA Northern Hemisphere, mWm^{-2}	TOA Southern Hemisphere, mWm^{-2}
Dec., Jan., Feb.	-0.1	-0.1	-0.1
Mar., Apr., May	-0.6	-1.2	-0.0
June, July, Aug.	-0.9	-1.6	-0.2
Sept., Oct., Nov.	-0.2	-0.1	-0.2
Annual Mean	-0.4	-0.8	-0.1

[16] Therefore, the global influence of visible ship tracks seems to be negligible. However, the ship tracks dilute in the surrounding cloud and might affect the clouds on larger scale that is not detectable with the satellite study presented here.

3. Conclusions and Discussion

[17] A semi-automated algorithm has been developed to derive a global distribution of ship tracks and to estimate the resulting radiative forcing (RF) from one year of ENVISAT-AATSR data. The algorithm first automatically selects scenes dominated by very low clouds in the marine boundary layer (VLC). In a second step, ship tracks are detected in the VLC scenes by visual analysis. Finally, the cloud optical properties of the ship tracks and the surrounding area within the selected scenes are used to estimate radiative changes on the local and global scale.

[18] High occurrence of VLC is found in regions at the west coasts of America and southern Africa and also between 30° and 60° in both hemispheres. Visual analysis of the pre-selected VLC scenes shows that most ship tracks occur in the North Pacific Ocean from May to July and in a smaller area on the west coast of southern Africa in August and September. Retrieved cloud optical properties are used to calculate the daily mean net radiation difference between the ship tracks and their surrounding areas, revealing changes between 0 and 100 Wm^{-2} . For some regions of the west coast of North America the RF due to ship tracks can be up to -0.05 Wm^{-2} . However, because of the small global coverage of ship tracks (0.002%), the global annual mean RF due to ship tracks is small (-0.4 mWm^{-2}). This contribution is negligible compared to the RF contributions of other ship emissions [Eyring et al., 2007; Capaldo et al., 1999].

[19] While previous studies have focused on local impacts of ship tracks [e.g., Durkee et al., 2000; Platnick et al., 2000; Schreier et al., 2006], this study presents the first global distribution of ship track coverage and the resulting change on the Earth's radiation budget. However, there are still some limitations for this analysis. For example the climatological relevance might be limited because only a single year of observations has been used and we have limited our data set to scenes with more than 20% coverage by VLC. A supplementary sample analysis shows a possible loss of 30% of ship tracks due to the pre-selection of the data. The error range for the RF calculations is estimated with $\pm 40\%$, mainly resulting from the retrieval of the cloud optical properties. Given these uncertainties, a range of -0.4 to $-0.6 \text{ mWm}^{-2} \pm 40\%$ can be given for the global annual mean radiative forcing of ship tracks. But despite these uncertainties, this study showed that ship tracks could possibly have an influence on the radiation budget of the Earth in some regions and seasons, and that the influence is negligible on a global scale. However, as ship tracks can mix with the ambient air and affect the surrounding clouds on a larger scale, improved global aerosol model studies or satellite trend analyses are needed to quantify the overall indirect aerosol effect due to ocean shipping.

[20] **Acknowledgments.** This work has been supported by the Helmholtz-University Young Investigators Group SeaKLIM, which is funded by the Helmholtz Association of German Research Centres, and the Deutsches

Zentrum für Luft- und Raumfahrt e.V. (DLR). We acknowledge support of the DFG project BU 688/8-1. AATSR data was provided by ESA through AOE.398 and we thank the ESA and the EO-help-desk for providing the data. Special thanks go to R. Büll, A. Lauer, R. Sausen, and U. Schumann from DLR and to J. P. Burrows from IUP Bremen for their help and fruitful discussions. Finally, thanks to the people from NASA for providing the ISCCP data.

References

- Albrecht, B. A. (1989), Aerosols, cloud microphysics, and fractional cloudiness, *Science*, *245*, 1227–1230.
- Cahalan, R. F., W. Ridgeway, and W. J. Wiscombe (1994), Independent pixel and Monte Carlo estimates of stratocumulus clouds, *J. Atmos. Sci.*, *51*, 3776–3790.
- Capaldo, K., J. J. Corbett, P. Kasibhatla, P. S. Fischbeck, and S. N. Pandis (1999), Effects of ship emissions on sulphur cycling and radiative climate forcing over the ocean, *Nature*, *400*, 743–746.
- Durkee, P. A., R. E. Chartier, A. Brown, E. J. Trehubenko, S. D. Rogerson, C. Skupniewicz, K. E. Nielsen, S. Platnick, and M. D. King (2000), Composite ship track characteristics, *J. Atmos. Sci.*, *57*, 2542–2553.
- Endresen, Ø., E. Sorgard, J. K. Sundet, S. B. Dalsøren, I. S. A. Isaksen, T. F. Berglen, and G. Gravir (2003), Emission from international sea transportation and environmental impact, *J. Geophys. Res.*, *108*(D17), 4560, doi:10.1029/2002JD002898.
- Entec UK Limited (2002), European Commission: Quantification of emissions from ships associated with ship movements between ports in the European Community, final report, Entec UK Ltd., London.
- Eyring, V., H. W. Köhler, J. van Aardenne, and A. Lauer (2005), Emissions from international shipping: 1. The last 50 years, *J. Geophys. Res.*, *110*, D17305, doi:10.1029/2004JD005619.
- Eyring, V., et al. (2007), Multi-model simulations of the impact of international shipping on atmospheric chemistry and climate in 2000 and 2030, *Atmos. Chem. Phys.*, *7*, 757–780.
- Han, Q., W. B. Rossow, J. Chou, and R. M. Welch (1998), Global variation of column droplet concentration in low-level clouds, *Geophys. Res. Lett.*, *25*(9), 1419–1422.
- Intergovernmental Panel on Climate Change (2007), *Climate Change 2007: The Physical Science Basis. Contribution of Working Group I to the Fourth Assessment Report of the Intergovernmental Panel on Climate Change*, edited by S. Solomon et al., Cambridge Univ. Press, New York.
- Kokhanovsky, A. A., V. V. Rozanov, E. P. Zege, H. Bovensmann, and J. P. Burrows (2003), A semianalytical cloud retrieval algorithm using back-scattered radiation in 0.4–2.4 μm spectral region, *J. Geophys. Res.*, *108*(D1), 4008, doi:10.1029/2001JD001543.
- Llewellyn-Jones, D., M. C. Edwards, C. T. Mutlow, A. R. Birks, I. J. Barton, and H. Tait (2001), AATSR: Global-change and surface-temperature measurements from Envisat, *ESA Bull.*, *105*, 20–21.
- Mayer, B., and A. Kylling (2005), Technical note: The libRadtran software package for radiative transfer calculations, description and examples of use, *Atmos. Chem. Phys.*, *5*, 1855–1877.
- Nakajima, T., and M. D. King (1990), Determination of the optical thickness and effective particle radius of clouds from reflected solar radiation measurements. Part I: Theory, *J. Atmos. Sci.*, *47*, 1878–1893.
- O'Dowd, C. D., M. H. Smith, I. E. Consterdine, and J. A. Lowe (1997), Marine aerosol, sea-salt and the marine sulphur cycle: A short review, *Atmos. Environ.*, *31*, 73–80.
- Platnick, S., P. A. Durkee, K. Nielsen, J. P. Taylor, S. C. Tsay, M. D. King, R. J. Ferek, P. V. Hobbs, and J. W. Rottman (2000), The role of background cloud microphysics in the radiative formation of ship tracks, *J. Atmos. Sci.*, *57*, 2607–2624.
- Rosenfeld, D., Y. J. Kaufman, and I. Koren (2006), Switching cloud cover and dynamical regimes from open to closed Benard cells in response to the suppression of precipitation by aerosols, *Atmos. Chem. Phys.*, *6*, 2503–2511.
- Rossow, W. B., and R. A. Schiffer (1991), ISCCP cloud data products, *Bull. Am. Meteorol. Soc.*, *72*, 2–20.
- Schreier, M., A. A. Kokhanovsky, V. Eyring, L. Bugiario, H. Mannstein, B. Mayer, H. Bovensmann, and J. P. Burrows (2006), Impact of ship emissions on microphysical, optical and radiative properties of marine stratus: A case study, *Atmos. Chem. Phys.*, *6*, 4925–4942.
- Twomey, S., H. B. Howell, and T. A. Wojciechowski (1968), Comments on anomalous cloud lines, *J. Atmos. Sci.*, *25*, 333–334.

H. Bovensmann and M. Schreier, Institute for Environmental Physics, University of Bremen, Otto-Hahn-Allee, D-28334 Bremen, Germany. (schreier@iup.physik.uni-bremen.de)

V. Eyring and H. Mannstein, Institut für Physik der Atmosphäre, Deutsches Zentrum für Luft- und Raumfahrt, Münchnerstrasse 20, D-82234 Oberpfaffenhofen, Germany.